Research Article | Vol. 25, No. 20 | 2 Oct 2017 | OPTICS EXPRESS 24033
Optics EXPRESS

Fast response and transparent optically isotropic liquid crystal diffraction grating

RAMESH MANDA,[1] SRINIVAS PAGIDI,[1] SURJYA SARATHI BHATTACHARYYA,[2] CHUL HO PARK,[1] YOUNG JIN LIM,[1] JIN SEOG GWAG,[3,4] AND SEUNG HEE LEE[1,*]

[1]*Applied Materials Institute for BIN Convergence, Department of BIN Convergence Technology and Department of Polymer Nano Science and Technology, Chonbuk National University, Jeonju, Jeonbuk, 561-756, Republic of Korea*
[2]*Asutosh College, 92, Shyamaprasad Mukherjee Road, Kolkata 700 026, West Bengal, India*
[3]*Department of Physics, Yeungnam University, 214-1 Dae-dong, Gyeongsan 712-749, South Korea*
[4]*sweat3000@ynu.ac.kr*
[*]*lsh1@chonbuk.ac.kr*

Abstract: We have demonstrated an electrically tunable less polarization sensitive and fast response nanostructured polymer dispersed liquid crystal (nano-PDLC) diffraction grating. Fabricated nano-PDLC is optically transparent in visible wavelength regime. The optical isotropic nature was increased by minimizing the liquid crystal droplet size below visible wavelength thereby eliminated scattering. Diffraction properties of in-plane switching (IPS) and fringe-field switching (FFS) cells were measured and compared with one another up to four orders. We have obtained a pore-type polymer network constructed by highly interlinked polymer beads at which the response time is improved by strong interaction of liquid crystal molecules with polymer beads at interface. The diffraction pattern obtained by transparent nano-PDLC film has several interesting properties such as less polarization dependence and fast response. This device can be used as transparent tunable diffractor along with other photonic application.

OCIS codes: (160.3710) Liquid crystals; (230.3720) Liquid-crystal devices; (230.1950) Diffraction gratings.

References and links

1. J. Chen and P.J. Bos. H. Vithana, and D. L. Johnson, "An electro-optically controlled liquid crystal diffraction grating," Appl. Phys. Lett. **67**(18), 2588–2590 (1995).
2. C. V. Brown, E. E. Kriezis, and S. J. Elston, "Optical diffraction from a liquid crystal phase grating," J. Appl. Phys. **91**(6), 3495–3500 (2002).
3. M. J. Rust, M. Bates, and X. Zhuang, "Sub-diffraction-limit imaging by stochastic optical reconstruction microscopy (STORM)," Nat. Methods **3**(10), 793–795 (2006).
4. I. Drevenšek-Olenik, M. Čopič, M. E. Sousa, and G. P. Crawford, "Optical retardation of in-plane switched polymer dispersed liquid crystals," J. Appl. Phys. **100**(3), 033515 (2006).
5. K. Pavani, I. Naydenova, S. Martin, J. Raghavendra, R. Howard, and V. Toal, "Electro-optical switching of liquid crystal diffraction gratings by using surface relief effect in the photopolymer," Opt. Commun. **273**(2), 367–369 (2007).
6. J. Sun, A. K. Srivastava, L. Wang, V. G. Chigrinov, and H. S. Kwok, "Optically tunable and rewritable diffraction grating with photoaligned liquid crystals," Opt. Lett. **38**(13), 2342–2344 (2013).
7. R. K. Komanduri, C. Oh, and M. J. Escuti, "Reflective liquid crystal polarization gratings with high efficiency and small pitch," Proc. SPIE **7050**, 70500J (2008).
8. H. C. Lin, M. R. Yang, S. F. Tsai, and S. C. Yan, "Gelator-doped liquid-crystal phase grating with multistable and dynamic modes," Appl. Phys. Lett. **104**(1), 011907 (2014).
9. N. Bennis, M. A. Geday, X. Quintana, B. Cerrolaza, D. P. Medialdea, A. Spadło, R. Dąbrowski, and J. M. Oton, "Nearly-analogue blazed phase grating using high birefringence liquid crystal," Opto-Elect. Rev. **17**(2), 112–115 (2009).
10. A. S. Chang, K. J. Morton, H. Tan, P. F. Murphy, W. Wu, and S. Y. Chou, "Tunable liquid crystal-resonant grating filter fabricated by nanoimprint lithography," IEEE Photonics Technol. Lett. **19**(19), 1457–1459 (2007).
11. W.-C. Hung, W.-H. Cheng, Y.-S. Lin, D.-J. Jang, I.-M. Jiang, and M.-S. Tsai, "Surface plasmons induced extra diffraction band of cholesteric liquid crystal grating," J. Appl. Phys. **104**(6), 063106 (2008).

#304089 https://doi.org/10.1364/OE.25.024033
Journal © 2017 Received 3 Aug 2017; revised 15 Sep 2017; accepted 18 Sep 2017; published 21 Sep 2017

Optics EXPRESS

12. H. C. Jau, T. H. Lin, R. X. Fung, S. Y. Huang, J. H. Liu, and A. Y. G. Fuh, "Optically-tunable beam steering grating based n azobenzene doped cholesteric liquid crystal," Opt. Express **18**(16), 17498–17503 (2010).
13. D. Xu, G. Tan, and S. T. Wu, "Large-angle and high-efficiency tunable phase grating using fringe field switching liquid crystal," Opt. Express **23**(9), 12274–12285 (2015).
14. J. Yan, Y. Li, and S. T. Wu, "High-efficiency and fast-response tunable phase grating using a blue phase liquid crystal," Opt. Lett. **36**(8), 1404–1406 (2011).
15. G. Zhu, J. N. Li, X. W. Lin, H. F. Wang, W. Hu, Z. G. Zheng, H. Q. Cui, D. Shen, and Y. Q. Lu, "Polarization-independent blue-phase liquid-crystal gratings driven by vertical electric field," J. Soc. Inf. Disp. **20**(6), 341 (2012).
16. B. Y. Huang, S. H. Lin, K. C. Lin, and C. T. Kuo, "Switchable Two-Dimensional Liquid Crystal Grating in Blue Phase," Cryst. **7**(6), 182 (2017).
17. G. Liao, S. Stojadinovic, G. Pelzl, W. Weissflog, S. Sprunt, and A. Jákli, "Optically isotropic liquid-crystal phase of bent-core molecules with polar nanostructure," Phys. Rev. E Stat. Nonlin. Soft Matter Phys. **72**(2), 021710 (2005).
18. S. J. Shin, N. H. Cho, Y. J. Lim, P. Nayek, S. H. Lee, S. H. Hong, H. J. Lee, and S. T. Shin, "Optically isotropic liquid crystal mixture showing high contrast ratio and fast response time," IMID Digest. 139, (2011).
19. S. Aya, K. V. Le, F. Araoka, K. Ishikawa, and H. Takezoe, "Nanosize-induced optically isotropic nematic phase," Jpn. J. Appl. Phys. **50**(5R), 051703 (2011).
20. N. Kim, D. Y. Kim, M. Park, Y. J. Choi, S. Kim, S. H. Lee, and K. U. Jeong, "Optically isotropic liquid crystal media formulated by doping star-shaped cyclic oligosiloxane liquid crystal surfactants in twin nematic liquid crystals," Soft Matter **11**(19), 3772–3779 (2015).
21. S. I. Yamamoto, T. Iwata, Y. Haseba, D. U. Cho, S. W. Choi, H. Higuchi, and H. Kikuchi, "Improvement of electro-optical properties on polymer-stabilised optically isotropic liquid crystals," Liq. Cryst. **39**(4), 487–491 (2012).
22. Z. G. Zheng, C. Wang, and D. Shen, "Dichroic-dye-doped polymer stabilized optically isotropic chiral liquid crystals," J. Mater. Chem. C Mater. Opt. Electron. Devices **1**(39), 6471–6478 (2013).
23. J. H. Yu, H. S. Chen, P. J. Chen, K. H. Song, S. C. Noh, J. M. Lee, H. Ren, Y. H. Lin, and S. H. Lee, "Electrically tunable microlens arrays based on polarization-independent optical phase of nano liquid crystal droplets dispersed in polymer matrix," Opt. Express **23**(13), 17337–17344 (2015).
24. Y. Haseba, H. Kikuchi, T. Nagamura, and T. Kajiyama, "Large Electro-optic Kerr Effect in Nanostructured Chiral Liquid-Crystal Composites over a Wide Temperature Range," Adv. Mater. **17**(19), 2311–2315 (2005).
25. Y. Tanabe, H. Furue, and J. Hatano, "Optically isotropic liquid crystals with microsized domains," Mater. Sci. Eng. B **120**(1), 41–44 (2005).
26. H. Khoshsima, H. Tajalli, A. G. Gilani, and R. Dabrowski, "Electro-optical Kerr effect of two high birefringence nematic liquid crystals," J. Phys. D Appl. Phys. **39**(8), 1495–1499 (2006).
27. S. W. Choi, S. I. Yamamoto, T. Iwata, and H. Kikuchi, "Optically isotropic liquid crystal composite incorporating in-plane electric field geometry," J. Phys. D Appl. Phys. **42**(11), 112002 (2009).
28. N. H. Cho, P. Nayek, J. J. Lee, Y. J. Lim, J. H. Lee, S. H. Lee, H. S. Park, H. J. Lee, and H. S. Kim, "High-performance, in-plane switching liquid crystal device utilizing an optically isotropic liquid crystal blend of nanostructured liquid crystal droplets in a polymer matrix," Mater. Lett. **153**, 136–139 (2015).
29. Y. C. Yang and D. K. Yang, "Electro-optic Kerr effect in polymer-stabilized isotropic liquid crystals," Appl. Phys. Lett. **98**(2), 023502 (2011).
30. S. Matsumoto, Y. Sugiyama, S. Sakata, and T. Hayashi, "Electro-optic effect, propagation loss, and switching speed in polymers containing nano-sized droplets of liquid crystal," Liq. Cryst. **27**(5), 649–655 (2000).
31. R. L. Sutherland, V. P. Tondiglia, L. V. Natarajan, T. J. Bunning, and W. W. Adams, "Electrically switchable volume gratings in polymer-dispersed liquid crystals," Appl. Phys. Lett. **64**(9), 1074–1076 (1994).
32. J. Kerr, "XL. A new relation between electricity and light: Dielectrified media birefringent," London, Edinburgh, and Dublin Philos. Mag. J. Sci. **50**(332), 337–348 (1875).
33. J. Yan, H. C. Cheng, S. Gauza, Y. Li, M. Jiao, L. Rao, and S. T. Wu, "Extended Kerr effect of polymer-stabilized blue-phase liquid crystals," Appl. Phys. Lett. **96**(7), 071105 (2010).
34. J. Yan, M. Jiao, L. Rao, and S. T. Wu, "Direct measurement of electric-field-induced birefringence in a polymer-stabilized blue-phase liquid crystal composite," Opt. Express **18**(11), 11450–11455 (2010).
35. L. Weng, A. Varanytsia, S. H. Lee, and L. C. Chien, "High-efficiency and fast-switching field-induced tunable phase grating using polymer-stabilized in-plane switching liquid crystals with vertical alignment," J. Phys. D Appl. Phys. **49**(12), 125504 (2016).
36. K. S. Ha, C. W. Woo, S. S. Bhattacharyya, H. J. Yun, H. S. Jin, Y. K. Jang, and S. H. Lee, "Analysis of optical bounce associated with two-step molecular reorientation in the fringe-field switching mode," Liq. Cryst. **39**(1), 39–45 (2012).
37. J. Yan, Y. Xing, and Q. Li, "Dual-period tunable phase grating using polymer stabilized blue phase liquid crystal," Opt. Lett. **40**(19), 4520–4523 (2015).

1. Introduction

Diffraction gratings are used in beam steering devices, optical inter-connecting devices, optical switches, diffraction filters, large screen projection display, holography, and three

Optics EXPRESS

dimensional displays due to the convenience of dynamic modulation of refractive index by external stimuli [1–3]. Variety of liquid crystal (LC) based phase gratings were proposed based on several different techniques viz. holographic [4], surface relief [5], rewritable [6], reflective [7], nanoparticle doped [8], blazed grating [9], nano-imprinting [10], cholesteric [11,12], large angle [13], etc.. The LC based phase grating formation requires a periodic modulation of refractive index in LC layers. Micron sized patterned electrodes are convenient for achieving periodic refractive index modulation and formation of grating structure. However, the diffracted light from traditional LC based phase gratings are found to be polarization dependent due to inherent anisotropic nature of LC molecules and the response time is limited due to large coherence length of LCs. Taking these disadvantages of traditional LC diffractors into account, tunable and fast response phase gratings capable of transmitting un-polarized beams in preferred directions are highly desirable.

To achieve aforementioned properties, the optically isotropic liquid crystal (OILC) diffractors such as polymer stabilized blue phase liquid crystals (PS-BPLC) are proposed [14–16]. However, it is also having disadvantages like requirement of precise temperature control during polymer stabilization process and hysteresis so that the PS-BPLC systems are limited to real device applications at present. An OILC can also be obtained by many techniques [17–23], among those the nanostructured polymer dispersed liquid crystal (nano-PDLC) are one of the best choices for achieving OILC [24–29]. Unlike PS-BPLC, where double twist cylinder in LC orientation forms cubic structure and thus the polymer network is required to exist in the disclination lines to stabilize the phase, the nano-PDLC possesses temperature insensitive electro-optic properties, wider curing temperature range, and wider phase than that of PS-BPLC. In addition, the nano-PDLC is optically transparent while the PS-BPLC reflects specific color due to Bragg reflection.

Here we have demonstrated experimental studies of polarization insensitive and sub-millisecond response OILC diffraction grating. The obtained grating is optically transparent in the visible wavelength regime. We have measured relative transmission change from zeroth order to higher order diffracted beams by applying an in-plane and fringing electric field. This device allows the dynamic control of the diffraction of light.

2. Theory

The nano-PDLC is optically isotropic, i.e. optically transparent, on macroscopic scale but holds short range ordering of LC [30,31]. The schematic switching mechanism of nano-PDLC is shown in the Fig. 1. The sample consists of encapsulated LC molecules in small droplet embedded in a polymer matrix. Orientation of LC in individual droplets is independent of their neighboring droplet. Hence the film does not offer synchronized phase shift to transmitted light. In presence of applied field, the LC molecules in droplets are enforced to follow periodic field lines. Thus light transmitted through the sample while subjected to such field encounters synchronized phase shift. This phenomenon is explained by the adoptive Kerr effect [32], expressed as, $\Delta n_{ind} = K\lambda E^2$, where Δn_{ind} is induced birefringence, K is Kerr constant, λ is wavelength of probing light, and 'E' is applied field. This phenomenon can be explained more precisely by extended Kerr equation and described as [33],

$$\Delta n_{ind}\left(E\right) = \Delta n_s \left\{1 - \exp\left[-\left(\frac{E}{E_s}\right)^2\right]\right\}, \tag{1}$$

where Δn_s is saturated birefringence and E_s is saturation field. Electric field induced refractive index Δn_{ind} reaches Δn_s when applied field (E) attains the saturation value. OILC is optically isotropic in field off state assumed to possess uniform effective refractive index (n_i), as shown in Figs. 1(a) and 1(c). When an electric field is applied through patterned electrodes, as shown in Figs. 1(b) and 1(d), the LC molecules having positive dielectric anisotropy reorient along

Optics EXPRESS

the field direction, and transmitted light experiences synchronized spatially modulated varying refractive indices with periodicity. The ordinary and extraordinary refractive indices represented as [34],

$$n_o(E) = n_i - \frac{\Delta n_{ind}(E)}{3},\ n_e(E) = n_i + \frac{2\Delta n_{ind}(E)}{3}, \tag{2}$$

where $n_e(E)$ is refractive index along the field direction while the $n_o(E)$ is the refractive index change orthogonal to field. The phase of incident light shifts ($\Delta\varphi$) along the cell gap (d), is represented by,

$$\Delta\varphi = \frac{2\pi}{\lambda}\left|\int_0^d n_o(E)\,dz - n_i d\right|, \tag{3}$$

The extended Kerr constant in nano-PDLC is dominated by anchoring energy of LC molecules at polymer interface instead of elastic energy [29]. Unlike other optically isotropic systems, the Kerr constant in polymer stabilized isotropic phase is highly dependent on the surface anchoring energy of each droplet.

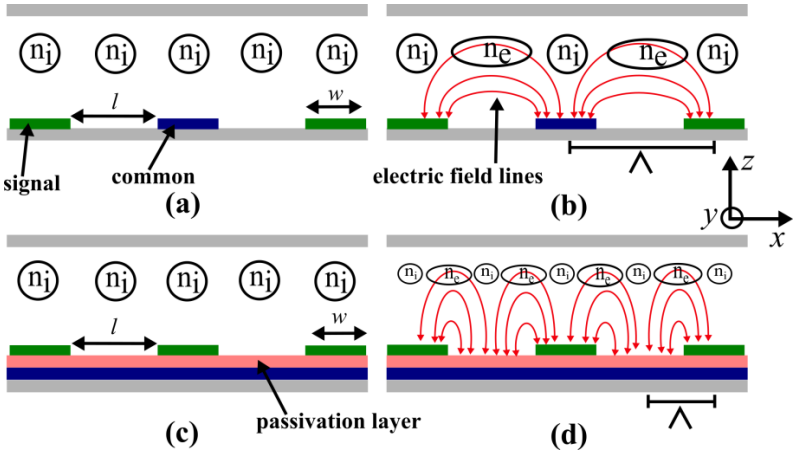

Fig. 1. Switching mechanism of OILC phase in IPS cell at (a) V = 0 & (b) V≠0, and FFS cell at (c) V = 0 & (d) V≠0. Pitch (Λ) of each cell is schematically represented.

The diffraction angle (θ_m) is governed by the pitch of the cell and the exact location of the diffracted spots can be calculated by the well-known grating equation expressed as,

$$\sin\theta_m = \frac{m\lambda}{n_{avg}\Lambda}, \tag{4}$$

where Λ is pitch of the grating, n_{avg} is average refractive index of the grating, and 'm' is the diffraction order (0, ± 1, ± 2, ± 3,…). θ_m is inversely proportional to the pitch (Λ). In IPS and FFS cells, the pitch of the grating is determined by inter-electrode space (l) and width (w) of the electrodes such that the patterned electrodes with pitch length results in modulation of refractive index profile, as shown in Fig. 1. In IPS cell, the pitch of the grating equals to 'w + l' which diffract the light accordingly when a field is applied. In contrary, the pitch of the FFS cell equals to (w + l)/2, which renders the diffraction angle double.

In diffractors, the phase shift is a linear function of the electrode periodicity. Experimentally, the θ_m is calculated from the following trigonometric relation,

$$\tan\theta_m = \frac{D_m}{L}, \tag{5}$$

Optics EXPRESS

where D_m is the separation between m^{th} and zeroth order, and L is the distance between the phase grating and the screen. The diffraction efficiency is defined as the ratio between the light intensity of m^{th} diffracted order at on-state and total intensity at off-state,

$$\eta_m(\%) = \frac{I_m(V)}{I_o} \times 100, \tag{6}$$

where $I_m(V)$ is intensity of m^{th} order subjected to driving voltage 'V', and I_o is total intensity of incident light at field-off state. The diffraction efficiency, i.e., the amount of light diffracted, is a function of the phase shift produced by LC molecules. The diffraction efficiency of LC device can be improved by optimizing the $d\Delta n$ value.

3. Experiment

In the present report, we have prepared a nano-PDLC phase by mixing high dielectric anisotropy nematic LC and two functionalized acrylate monomers. We have used MLC-2053 ($\Delta\varepsilon$ = 46.2, n_e = 1.7472, n_o = 1.5122, Δn = 0.235 at 589.3nm, K_1 = 13.2 pN, K_2 = 6.5 pN, K_3 = 18.3 pN, rotational viscosity (γ) = 123 mPa·s, from Merck Advanced Technology, Korea) as nematic LC, Trimethylolpropane Triacrylate (TMPTA, Sigma-Aldrich) and Pentaerythritol Tetraacrylate (PETTA, Sigma-Aldrich) as monomers. Small amount of photo-initiator, Irgacure-907, was added to the mixture to initiate the radical polymerization. The prepared sample consists of 46 wt% of MLC2053, 26 wt% of TMPTA, 27 wt% of PETTA, and 1 wt% of Irgacure-907. The crystallization and clearing temperature of MLC-2053 is –10 °C and + 86 °C, respectively.

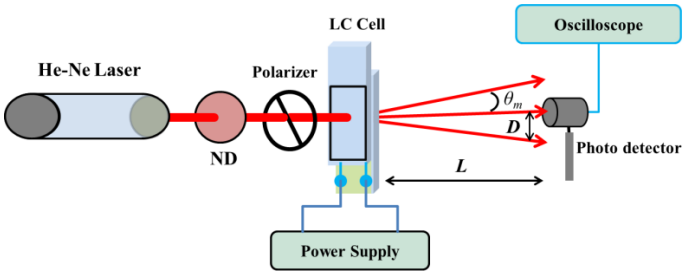

Fig. 2. Pictorial representation of experimental set up for electro-optic measurements of diffraction grating. ND is neutral density filter. The polarizer sets polarization direction perpendicular to the long ITO electrode strip to select the TM polarization.

The polarizing optical microscope (Nikon, ECLIPSE E600, Japan) attached with CCD camera (Nikon, DXM 1200), was used to characterize isotropic phase, and switching of nematic mixture. The diffraction efficiency was determined by monitoring transmittance change of He-Ne laser (λ = 632.8 nm) in response to 1 kHz square wave voltage applied to nano-PDLC film. The transverse magnetic (TM) mode was chosen to measure diffraction efficiency. In this experiment, the distance between the cell and screen was fixed to 72 cm to realize the far field diffraction. The experimental set-up used to study the diffraction behavior of the grating is shown in the Fig. 2, described elsewhere [35].The change in transmittance due to diffraction as a function of applied field is recorded by photo-detector and stored in digital storage oscilloscope (Tektronix, DPO2024B). Snapshots of diffraction spots on screen placed behind the cell are also recorded simultaneously using digital camera (Samsung, NX1000). We have experimentally determined the polarization states of various orders of diffracted beam by placing analyzer behind the cell and measuring resultant intensity change by photodiode. The wavelength-dependent transmittance was measured by using an UV-Visible spectroscopy (SCINCO, S-3100) from ultraviolet to near infrared region. Finally, the obtained monomer network was characterized by the field emission scanning electron microscope (FESEM).

Optics EXPRESS

The IPS cell consists of comb-like ITO stripes of 4 μm width (*w*) and 4 μm inter electrode space (*l*) patterned on bottom substrate with no electrodes on top substrate. The FFS cell consists of pixel and common electrodes separated by a thin passivation layer where the electrode width (*w*) and space (*l*) between the pixel electrodes are 3.5 μm and 4.5 μm, respectively. The cell gap for IPS and FFS were fixed to 5 μm. Test cells were filled with homogeneous mixture of LC and monomers, and exposed to 300 mW/cm^2 intense UV light with 365 nm wavelength for 10 minutes at 90 °C. As curing temperature considerably affects phase separation; optimum curing conditions are necessary to obtain intended randomly oriented small sized LC droplets embedded in polymer matrix. We have polymerized the film at isotropic temperature, 90 °C, to obtain optimum phase separation and nullify anisotropic effects of LC.

4. Results and discussion

We intend to induce periodic phase modulation of transmitted light through nano-PDLC film with sharp boundaries where spatial distribution is fixed by patterned electrodes. The photographic images of the recorded diffraction pattern as a function of applied voltage have been illustrated in the Fig. 3. The obtained transmission intensity is mostly concentrated at center of the grating pattern in field off state and spare amount of diffracted light appears symmetrically on both sides of 0th order due to refractive index mismatch between the electrode region and non-electrode regions in IPS cell and refractive index mismatch between single ITO layer and double ITO layers in FFS cell. However, when the electric field is applied, the LC molecules reorient along the field direction due to in-plane field in IPS and fringe field in FFS cell thereby causing periodic modulation in respective LC director profile. Hence, transmitted coherent laser beam encounters spatially periodic phase modulation, resulting in constructive interference patterns at specified angles by following Eq. (4) where the periodicity is described by nano-PDLC deformation guided by respective in-plane and fringe field and n_{avg} is average refractive index of nano-PDLC sample as discussed earlier. Consequently, transmission intensity obtained in 0th order decreases and beam is deviated symmetrically to various higher orders increase with increasing field strength. Total 4 diffraction orders could be distinguished by naked eyes at on-state symmetrically distributed on either side of 0th order. As a voltage increases from 0 V to 40 V, the light intensity is transferred from 0th order to all higher orders in IPS cell, Fig. 3(a). In contrary, the light intensity is transferred from 0th order to 2nd and 4th orders in FFS cells, Fig. 3(b), indicating that diffraction angle is doubled in FFS cell compared to IPS cell.

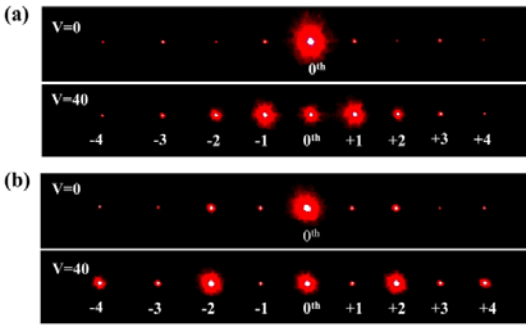

Fig. 3. The diffraction pattern recorded for OILC phase switching with, (a) IPS, and (b) FFS cells. The incident polarization direction is perpendicular to the long electrode to select the TM polarized light. Corresponding dynamic responses of the IPS (see Visualization 1) and FFS (see Visualization 2) are also recorded.

We have determined relative change in intensity of FFS and IPS diffraction grating and its corresponding results are illustrated in the Fig. 4(a). The screen behind the cell was replaced

Optics EXPRESS

by photo-detector connected to digital oscilloscope. Electric field appears to affect alternating orders of diffracted beam in FFS in contrast with IPS diffractor such that the transmission intensity appears to shift from 0th order to 2nd and 4th orders in FFS cell with increasing applied electric field. The mechanism behind this selective intensity transfer in FFS cell is local minimum director profile of nano-PDLC matrix where characteristic length scale determined by l and w. Experimental results exhibit different field-driven diffracting behavior for IPS and FFS mode. Diffraction angle (θ_m) and diffraction efficiency (η_m) are measured by using Eqs. (5) and (6), respectively and the obtained results are summarized in the Table 1. The intensity of higher order at field-off state was neglected. The maximum diffraction efficiency of IPS and FFS cells are found to be 33% and 31%, respectively. The small decrease, 2%, in diffraction efficiency in FFS cell is due to wider $w + l$ compared to cell gap (d). The measured diffraction angles are well consistent with theoretical values in both IPS and FFS cells.

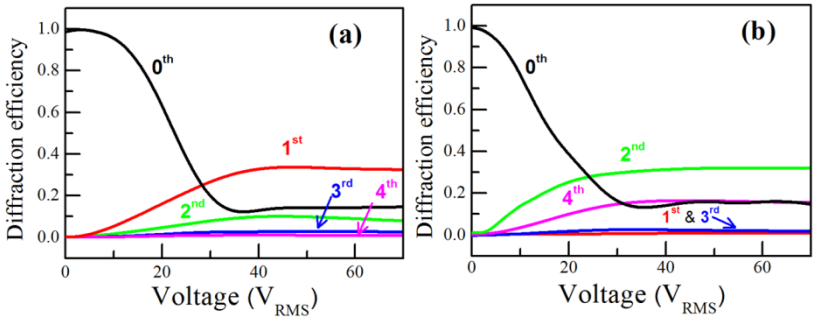

Fig. 4. The relative transmittance change and diffraction efficiency as a function of applied voltage, (a) IPS, and (b) FFS cells. The diffraction efficiency is defined by Eq. (6).

Table 1. Measured diffraction angle (θ_m) and diffraction efficiencies (η_m) of IPS and FFS based OILC phase grating. He-Ne laser (λ = 632.8 nm) was used as light source.

Diffraction Order	IPS at 40 V				FFS at 40 V			
	D_m (cm)	η_m (%)	θ_m (°)	θ_m (°)[a] (theoretical)	D_m (cm)	η_m (%)	θ_m (°)	θ_m (°)[a] (theoretical)
1st	6.9	33	5.4	5.5	6	31	4.7	4.9
2nd	14	13	11.0	11.1	12.3	1	9.6	9.9
3rd	21.6	7	16.6	16.9	18.2	14	14.9	14.9
4th	27.5	1	20.8	22.8	24.4	2	20.1	20.2

[a]angle calculated from theoretically obtained grating equation Eq. (4).

The results of response time measurement for both IPS and FFS cells are shown in Fig. 5. The change in transmittance in response to 40 V and 1 kHz square wave is depicted. The rise and decay times are defined as 10% to 90% transmittance change while applying and removing the field, respectively. The measured rise and decay times are ~0.8 ms and ~2.9 ms for IPS, respectively. Measured rise and decay times for FFS are 0.8 ms and 1 ms, respectively. The decay time of FFS cell is approximately three times faster than IPS cell. The FFS cell provides fast response and large angle diffraction but the relative diffraction efficiency is reduced by ~2%. The IPS cell provides high diffraction efficiency but small diffraction angle and slow response compared to FFS cell.

Since the rise response time is strongly influenced by the applied field in both cases, the sub-millisecond rise response time is attributed from the strong applied field 10 V/μm. The decay response time is mainly associated with director relaxation mechanism which is strongly controlled by visco-elastic constants (the ratio of rotational viscosity to effective elastic constant) γ/K_{eff} if we assume the size of LC droplets and surface anchoring strength

Optics EXPRESS

between LC and polymer network are similar in both kind of cells. In IPS cell, the LC director inside droplets reorients along in-plane electric field direction such that elastic deformation of LC director is mainly twist deformation (K_2). Moreover, electric field induced twist deformation diminishes in LC droplet along cell thickness from bottom to top surface. Unlike IPS cell, the fringe field like parabolic shape is generated between electrode and the field intensity near electrode surface is much stronger in the FFS than IPS. Consequently, the LC directors experiences mainly tilt and bend, and then twist deformation, that is, the deformation of LC directors inside droplets is associated with splay K_1, twist K_2, and bend K_3 elastic constants. Therefore, the effective elastic constant is approximately replaced by (K_1 + K_2 + K_3)/3 if three deformations contribute equally in the FFS cell whereas only K_2 contributes in IPS. The magnitude of elastic constants of LC mixture tested here appears according to following relation $K_3 > K_1 > K_2$. Therefore, the faster decay time in the FFS cell might be from larger effective elastic constant compared to that in the IPS cell. In addition, the mentioned nano-sized droplets whose size up to few hundreds of nanometer is also another reason which makes LC relaxation faster because the cell gap is replaced by droplets size. Regarding the optical bounce in decay time of FFS cell, in conventional FFS cell [36] with homogenous alignment at an initial state, the LC with positive dielectric anisotropy twists along horizontal component of a fringe-field direction and simultaneously LC director tilts at high angle along the fringe field in a voltage-on state. When applied voltage is turned off, the LC director first tilts and then un-twisted back to an initial state sequentially. During such a two-step transition, a transmittance increases instantaneously giving rise to an optical bounce because the decrease of a tilt angle of LC director increases its twist level. The physical explanation is applicable even for OILC cell. In a voltage-on state, the LC directors inside droplets experience tilt deformation mainly along fringe-field and when the voltage is turned off, the tilt relaxes initially because K_1 and K_3 is larger than K_2, then the effective retardation at a normal direction becomes larger instantaneously, resulting in an increase in transmittance called optical bounce.

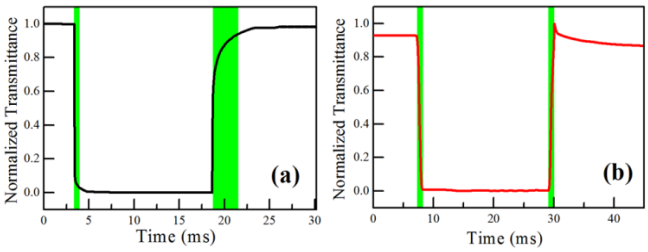

Fig. 5. Response times of the zeroth orders of (a) IPS, and (b) FFS cells.

The procedure followed in revealing the dependence of transmission intensity on polarization direction of incident beam over OILC diffractor is described below. The beam incident on test cell made linearly polarized using polarizer placed between neutral density filtered incident He-Ne laser beam and cell. Test cells placed in above mentioned configuration were rotated from 0° to 90° and transmission intensity was recorded using photodiode. Hence, experimentally obtained variation of intensity of diffracted beam for 1st order in IPS cell and 2nd order in FFS cell are depicted in the Figs. 6(a) and 6(b), respectively. The intensity of the diffracted light is not remained invariant on sample rotation in the cell plane at field-on state. One could observe a noticeable change in intensity both for IPS and FFS cells, thus they are not completely polarization independent rather appears less sensitive to polarization state of incident light. As one could anticipate from refractive index profile along x-direction perpendicular to electrodes in Figs. 1(b) and 1(d), the incident linearly polarized light encounters n_i above electrode and n_e between electrode, where n_e is larger than n_i. However, when polarization state of incident beam rotates by 90°, it experiences n_i above electrode and n_o between electrode, having $n_i > n_o$. Consequently, the

Optics EXPRESS

incident beam polarized either in *xz* or *yz* plane experiences periodic change in optical path. However, the relative sign of optical path reverses depending on a direction of polarization of incident beam, resulting in some level of polarization dependence in transmitted beam. In fact, such a refractive index profile renders the diffractor behave like lens but significant changes in optical path depends on direction of polarization of incident beam in either *xz* or *yz* plane. Present explanation is clearly demonstrated using polarizing optical microscopic image shown in inset of figures Fig. 7(a) such that the bright lines change to dark lines depending on polarization state of incident beam.

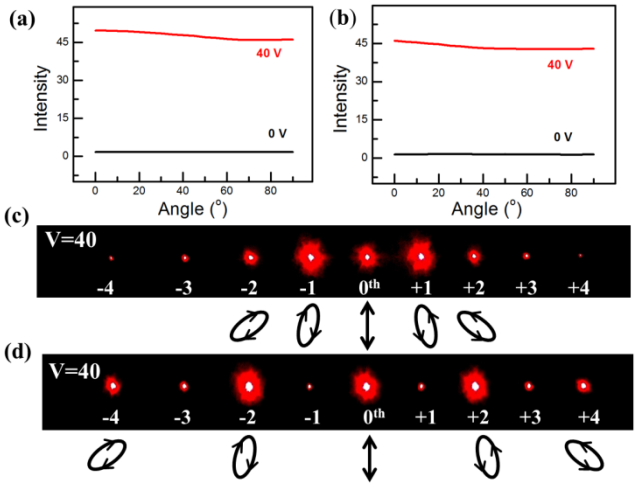

Fig. 6. Polarization dependency of the diffracted beam in (a) IPS cell's 1st order, and (b) FFS cell's 2nd order. Polarizations states of the various diffraction orders of (c) IPS cell and (d) FFS cell.

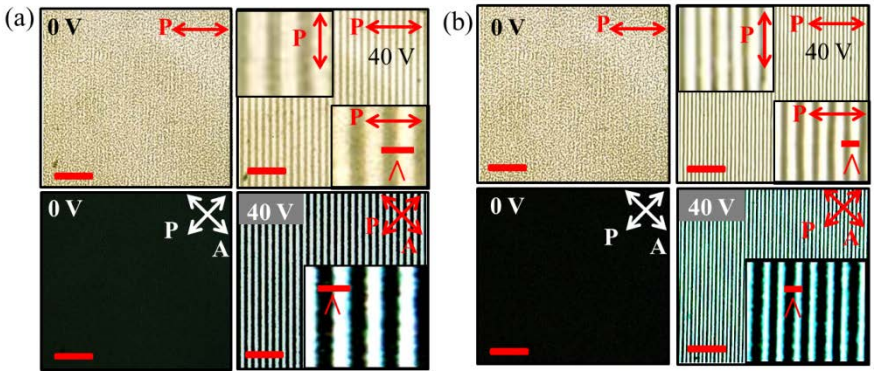

Fig. 7. POM images of (a) IPS and (b) FFS cells filled with nano-PDLC. Top row represents images with single polarizer used in which polarization direction of an incident light is perpendicular to the long ITO electrode. Bottom images represent texture under crossed polarisers in which polarization direction of an incident light is 45° with respect to long ITO electrode. Here, the pitch (Λ) is clearly shorter in FFS than IPS cell. Represented scale bar is 40 μm.

We have determined polarization states of few higher order diffracted beams in both IPS and FFS cell as shown in Figs. 6(c) and 6(d), respectively. The beam incident on test cell was linearly polarized using polarizer placed between neutral density filtered incident He-Ne laser beam and cell. To determine the polarization state of each diffracted beam, the analyzer was placed behind the cell. The polarization state is confirmed by rotating the analyzer in clockwise direction and measuring resultant change in intensity using photodiode. All the

Optics EXPRESS

reported polarization states are determined while OILC sample is subjected to 40 V. The polarization states of spatially distributed diffracted orders found to be slightly different from each other. The polarization state of 0th order remains unaffected in both IPS and FFS cells while remaining orders are elliptically polarized and also the major axis of the elliptically polarized light in higher order deviates more from initial polarization direction. In addition, the polarization states in left and right side of 0th order possesses mirror symmetric to each other.

Figure 7 shows POM images, which allows us to analyze the director distribution under in-plane and fringe field switching. The bright region at field-on state where single polarizer was employed is due to modulation of refractive index between electrode and non-electrode regions, as already explained above. The refractive index profile between the electrode strips would be analogue to parabolic shape of an electric field in both devices such that the refractive index at mid-point between electrodes, near the electrodes, and above electrode will be largest, intermediate, and smallest for *xz*-polarized light in the IPS cell, rendering the diffractor behaves as lens. On the other hand, for *yz*-polarized light, the relationship of amplitude of refractive index along *x*-direction is reversed. This is clearly observed in inset figures of Figs. 7(a) and 7(b) such that the bright lines become dark lines depending on direction of polarization state of incident light. To check the transparency of the OILC cells without causing scattering, the cells were rotated while confined between crossed polarizers. As expected, an excellent dark state without a transmitted light is achieved in all directions, as indicated in dark POM images in Fig. 7. In a voltage-on state, we could achieve uniform brightness between electrodes for the IPS cell and the edge of patterned electrode for the FFS cell. This is the direct experimental verification of the periodic refractive index change of LC under influence of an electric field. Close observation of the images suggests that there is no minimal brightness or dark line at center of the two adjacent electrodes in IPS, while minimum brightness or dark line appears at center of patterned electrodes and also at the mid-point between electrodes in FFS, confirming the difference in pitch of the grating Λ in both devices.

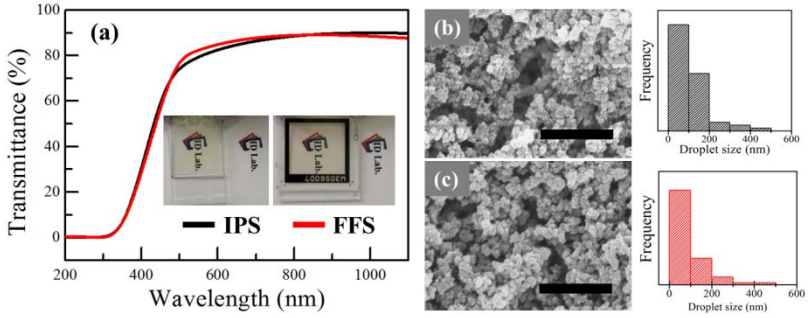

Fig. 8. (a) Wavelength dependent transmittance curves for IPS and FFS cells. The photograph images of the cells as shown in inset. Obtained polymer structure of nano-PDLC film prepared in (b) IPS and (c) FFS cell. The represented scale bar is equal to 500 nm.

We have measured the wavelength dependent transmittance from ultra-violet to near infrared regions for either kind of test cells, and obtained transmission spectrum is shown in Fig. 8(a). The wavelength dependent transmittance evidences transparency of the OILC phase in IPS and FFS cells. The measured maximum transmittance is as high as ~85%. We have also observed the transmittance of cells by capturing photographic images, inserted in Fig. 8(a). The background images are clearly visible in both cells, indicating the obtained film is transparent.

Finally, the polymer network structure characterized by FE-SEM. The two substrates of cells were separated by sharp edged scalpel blade after extraction of LC molecules by keeping in hexane for 48 hours. Films were carbon coated and images taken perpendicular to the

Optics EXPRESS

substrate. The obtained FE-SEM images of IPS cell and FFS cell are shown in Figs. 8 (b) and 8(c), respectively. We obtained a pore-like polymer network constructed by highly interlinked polymer beads. It is obvious that the shape of the pore structure is deviating from spherical shape. The size and distribution of the pore was estimated by Image-J software. One could notice that the average size of the pore is below 300nm, which resulted in scattering free film, so that the film acts as an optically isotropic medium. The fast response time might be also due to a strong coupling interaction of LC molecules with polymer beads. The diffraction pattern obtained by transparent OILC film has several interesting properties such as transparent, less sensitive to polarization state of incident beam and fast response. This device can be used as photonic applications such as transparent Fresnel lens, transparent holography and also a potential candidate for see-through transparent display.

5. Conclusion

We have demonstrated a transparent and tunable LC diffractor constructed with IPS and FFS cells. The measured response times are 3.7 ms and 1.8 ms for IPS and FFS cells, respectively, which are competitive records among recent related reports [13,35,37]. The interlinked polymer beads formed as pore-type structure which could exert the strong interaction with LC molecules could be the reason for fast response. The optically isotropic phase was obtained by the phase separation of monomers under controlled UV irradiation dynamics. Film is optically transparent in the visible wavelength range. The IPS and FFS diffraction efficiencies were studied quantitatively up to four orders. The sample is found to be less sensitive to polarization state of incident beam. The experimental studies show that the spatially varying phase shift makes the nano-PDLC diffractor is a promising candidate for fast response photonic and transparent display applications.

Acknowledgments

This research was supported by the Basic Science Research Program through the National Research Foundation of Korea (NRF) funded by the Ministry of Education (2016R1A6A3A11930056 and 2016R1D1A1B01007189).